Electronic Supplementary Material (ESI) for Journal of Materials Chemistry A.

Electronic Supplementary Material

2.5 V Salt-in-water supercapacitors based on alkali type double salt/carbon composite Anode

Tianfeng Qin,[a] Zhiyuan Xu,[a] Zilei Wang,[a] Shanglong Peng,[a] Deyan He,*[a]

Key Laboratory for Magnetism and Magnetic Materials of the Ministry of Education, School of Physical Science and Technology, Lanzhou University, Lanzhou 730000, P.R. China.

E-mail: hedy@lzu.edu.cn.

Fig. S1 The OCC (left) and ATDS@OCC (right) with a size of 4.5 X 4.5 cm^2 to demonstrate the scalability of the method.

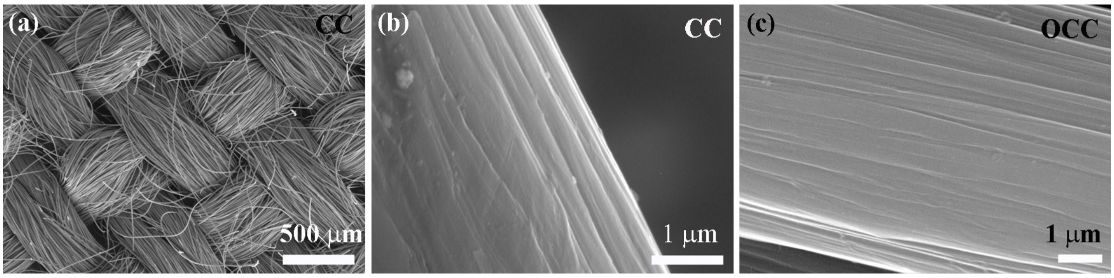

Fig. S2 SEM images of (a, b) CC and (c) OCC.

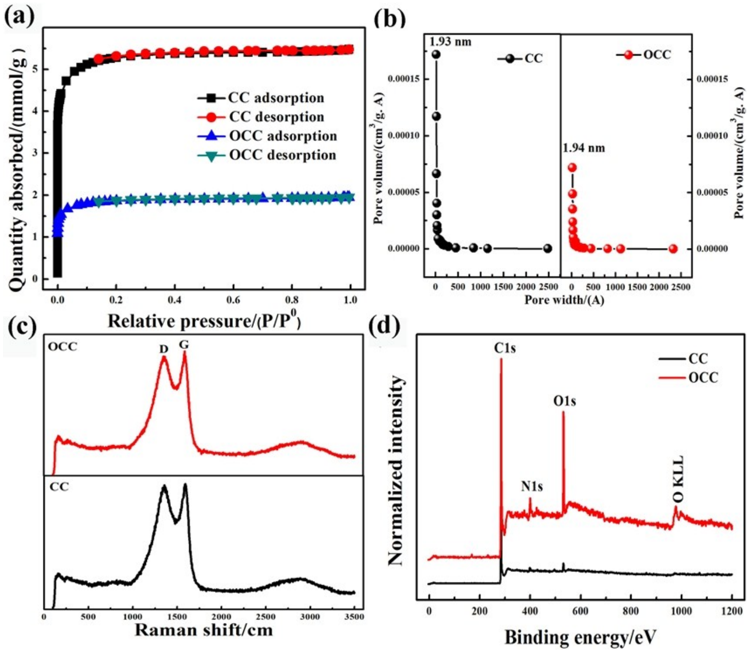

Fig. S3 (a) N_2 adsorption/desorption isotherms, (b) pore width distribution, (c) Raman spectra and (c) XPS spectra of CC and OCC. BET surface areas are 360 m^2 g^{-1} and 127 m^2 g^{-1}, and pore volumes are 0.19 cm^3 g^{-1} and 0.07 cm^3 g^{-1} for CC and OCC, respectively.

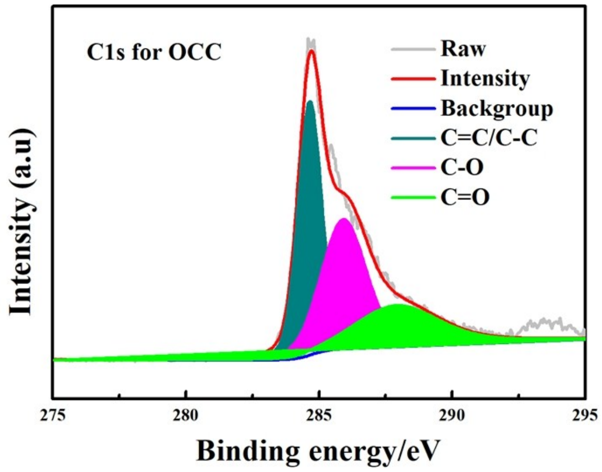

Fig. S4 C1s narrow XPS spectrum of OCC, which consists of three peaks of C=C/C-C, C-O and C=O. [1-3]

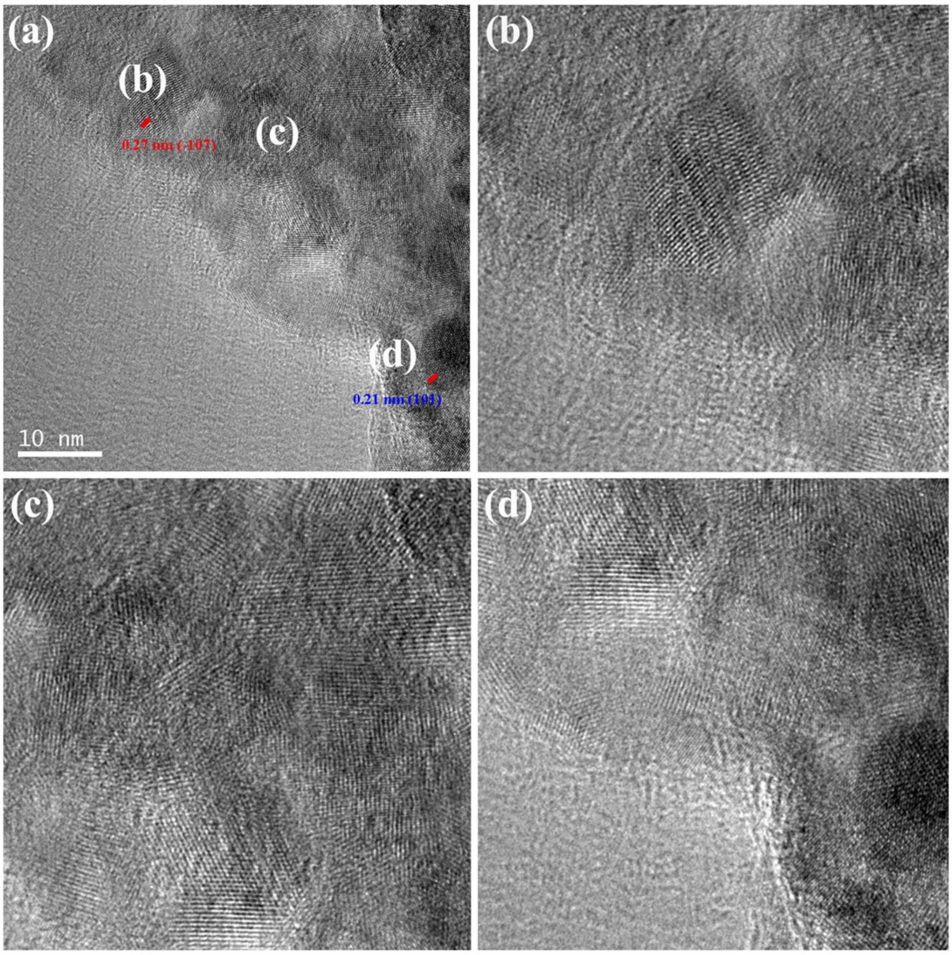

Fig. S5 (a) High-resolution TEM image of ATDS. (b-d) The partial magnification images of (a).

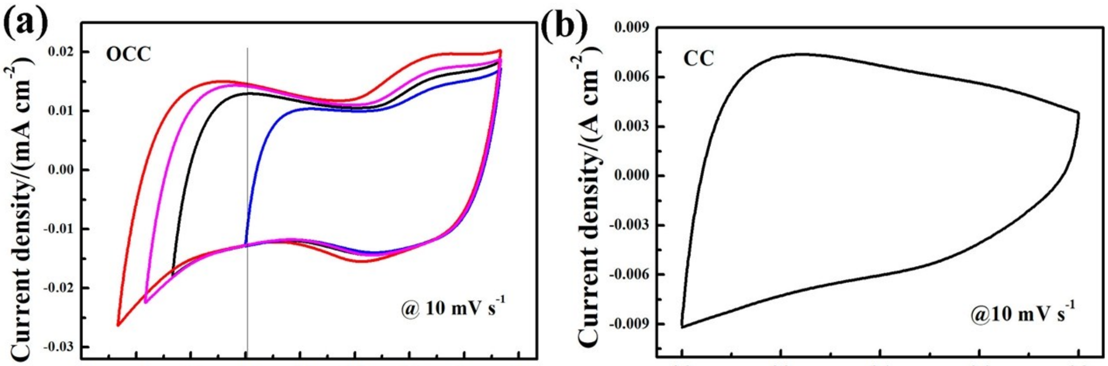

Fig. S6 CV curves tested in a three-electrode configuration of (a) OCC as negative electrode and (b) CC as positive electrode.

Cyclic voltammetry (CV) method is firstly employed to show the characteristic of the wide potential range for negative OCC electrode and CC as positive electrode in 1 M Na_2SO_4 aqueous electrolyte. For the di-hydrogen evolution shown in Fig. S4a, the theoretical potential in 1 M Na_2SO_4 aqueous solution is -0.59 V *vs* SCE, e.g., the reduction potential of water (the calculation is illustrated in Note S1 below). If the negative potential limit was above the reduction potential of water during cathodic sweep, CV curve would indicate the characteristic of double-layer capacitor. In contrast, if it was below -0.59 V *vs* SCE, the water solvent in electrolyte would be reduced, in which the double-layer would be produced accompanying with the pseudo-capacitance originated from the reversible sorption of hydrogen in pores of carbon cloth. [3, 4] For CV curves of OCC, an obviously upward shift is observed during the anodic sweep due to the electrochemical oxidation of hydrogen stored in pores. [3, 5] Thus, the reduction/oxidation of hydrogen may contribute the pseudo-capacitance to the total capacitance of OCC. And much more basic functional groups such as C-O and C=O on the in-wall of pores in Fig. S3 can inhibit the evolution of H_2, [6, 7] which is benefit for the expand of negative potential range. Besides, positive CC electrode with high specific surface area and rich O functional groups (Fig. S2) can operate in the potential range from 0 V to 0.8 V *vs* SCE in Fig. S4b. Finally, we estimate that the potential window of OCC//CC aqueous supercapacitor is about 2.1 V.

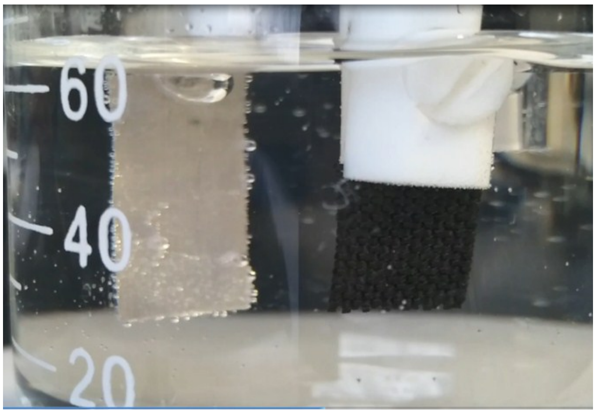

Fig. S7 The screenshot of the recorded short video at 12th second (charging to -1.3 V) to show that no bubbles were observed on the surface of black OCC as negative electrode. The corresponding testing curve at a potential window of -1.3 - 0.8 V is shown in Fig. S6 (a).

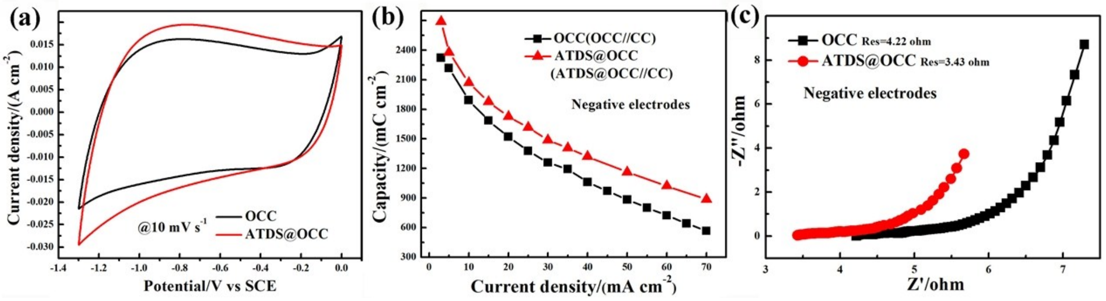

Fig. S8 Electrochemical properties of OCC cycled in OCC//CC and ATDS@OCC cycled in ATDS@OCC//CC. (a) CV curves at 10 mV s^{-1}, (b) capacity as a function of current density and (c) Nyquist plots.

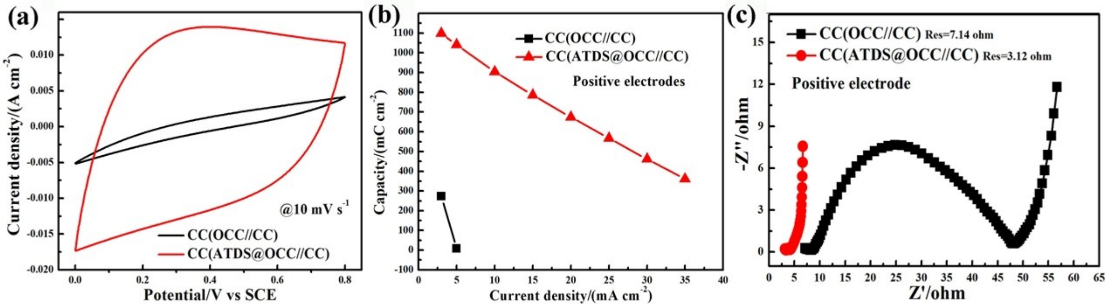

Fig. S9 Electrochemical properties of the CC positive electrodes cycled in OCC//CC and ATDS@OCC//CC. (a) CV curves at 10 mV s^{-1}, (b) capacity as a function of current density, and (c) Nyquist plots.

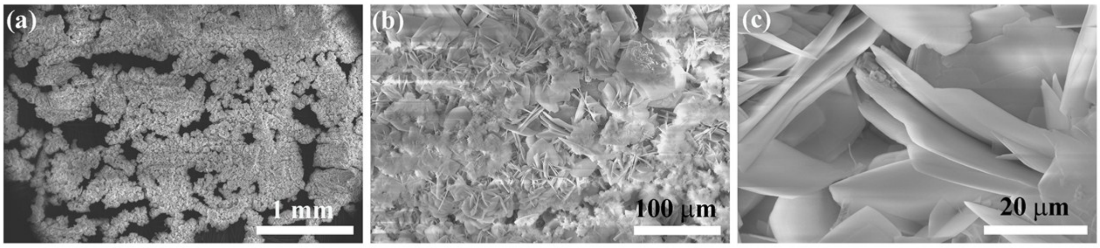

Fig. S10 Different magnification SEM images of the cycled ATDS@OCC in the ATDS@OCC//CC supercapacitor.

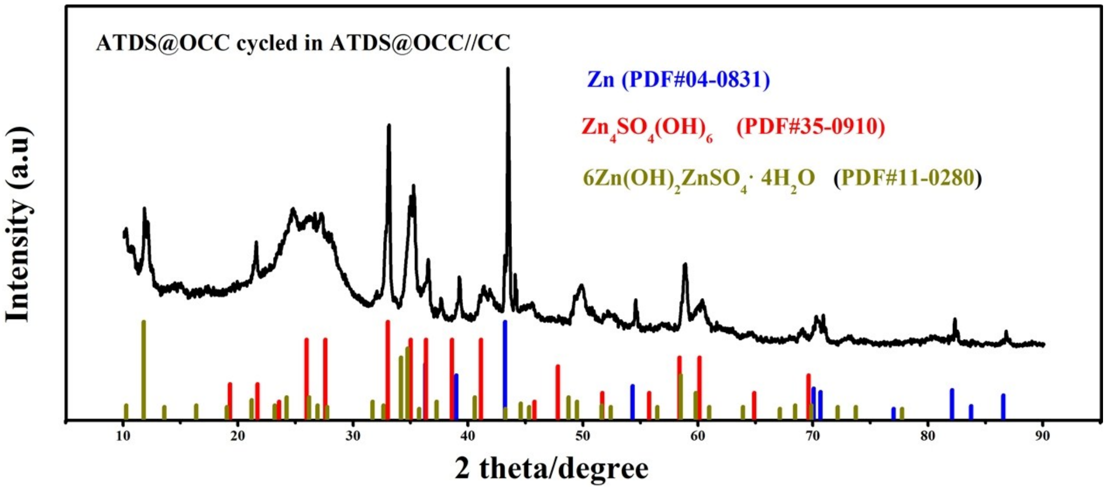

Fig. S11 XRD pattern of the cycled ATDS@OCC in the ATDS@OCC//CC supercapacitor.

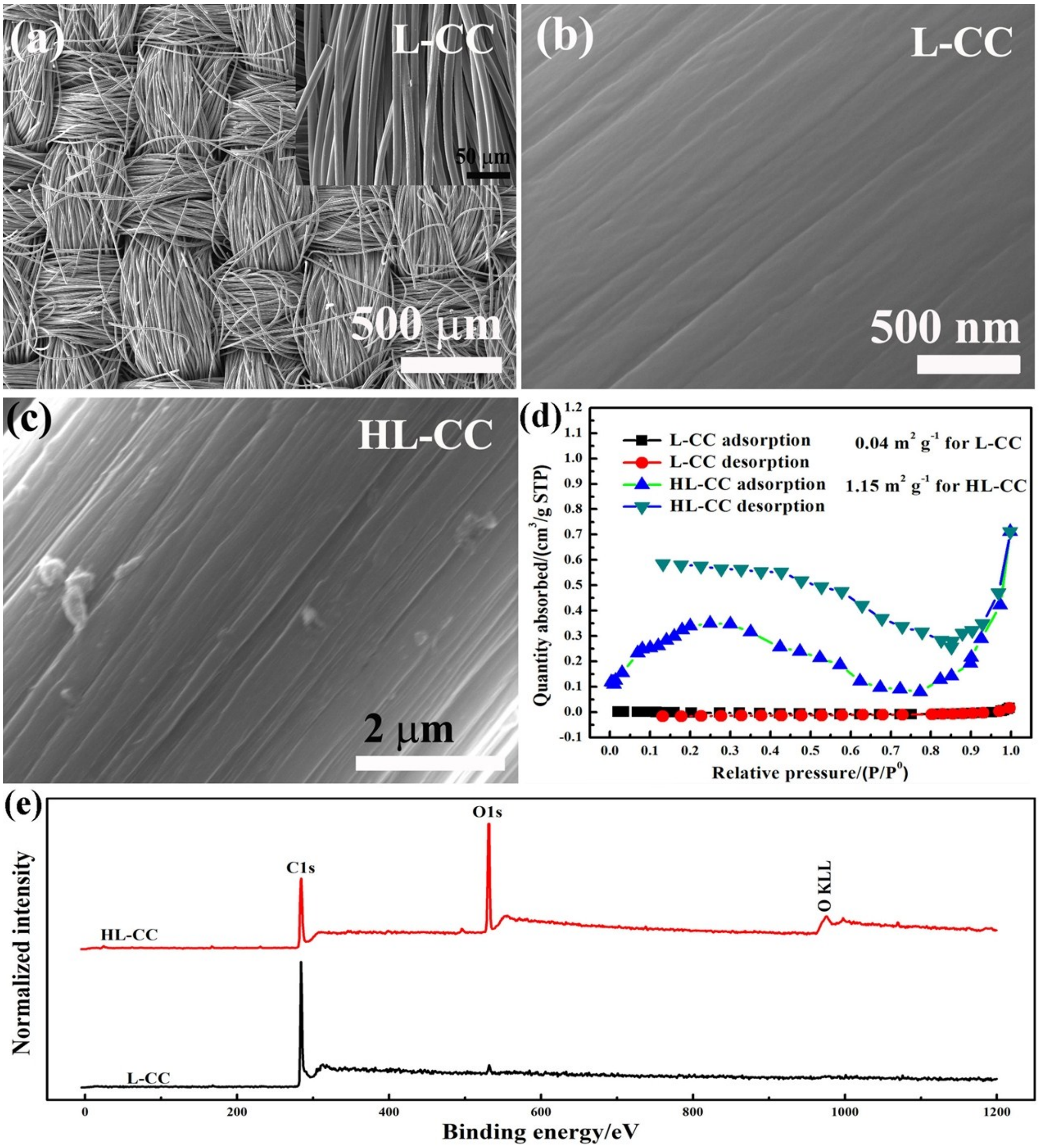

Fig. S12 (a, b) SEM images of low surface area carbon cloth (L-CC) purchased from Taiwan Tanneng. (c) SEM image of HL-CC obtained through electrochemical oxidation of L-CC in concentrated H_2SO_4. (d) N_2 adsorption/desorption isotherms of L-CC and HL-CC. (e) XPS spectra of L-CC and HL-CC. The electrochemical oxidation was carried out using a three-electrode configuration, in which SCE and Pt plate were employed as reference electrode and counter electrode, respectively. 3 V and 15 min were selected to start the process.

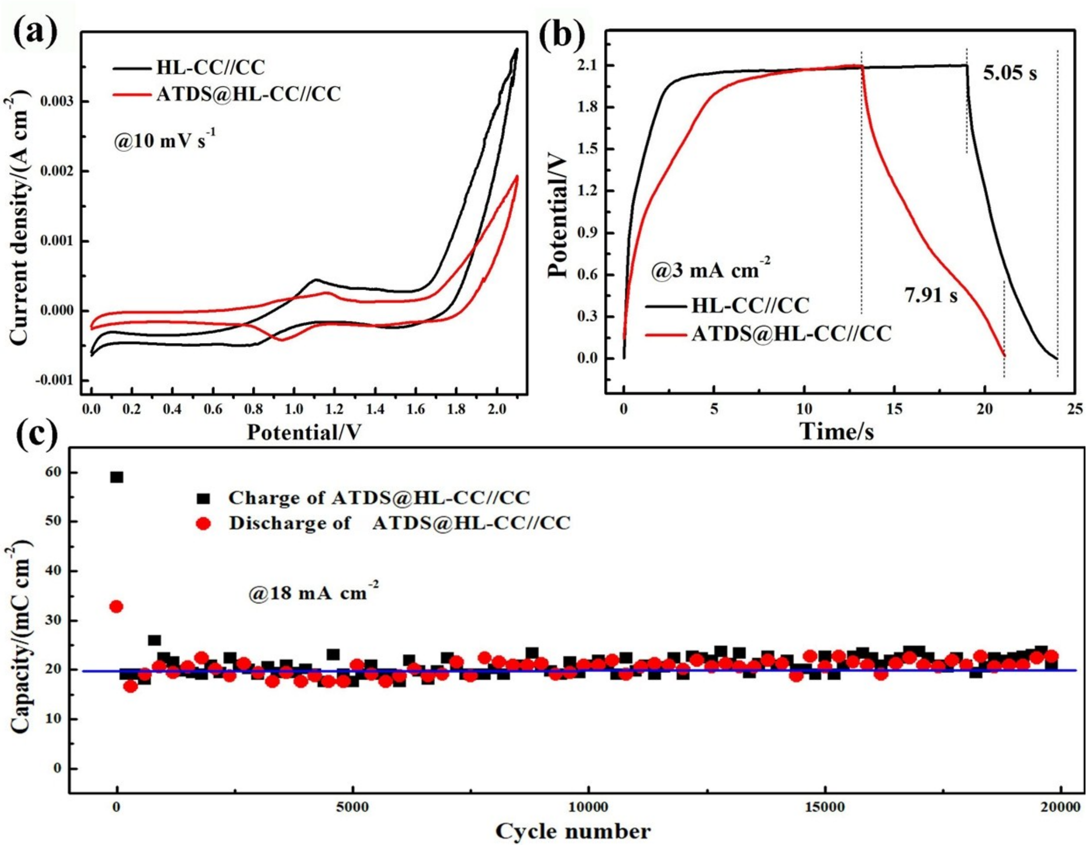

Fig. S13 (a) CV and (b) GCD curves of HL-CC//CC and ATDS@HL-CC//CC supercapacitors. (c) Long-term cycling stability of ATDS@HL-CC//CC supercapacitor with a voltage range from 0 V to 2.1 V at 18 mA cm^{-2}.

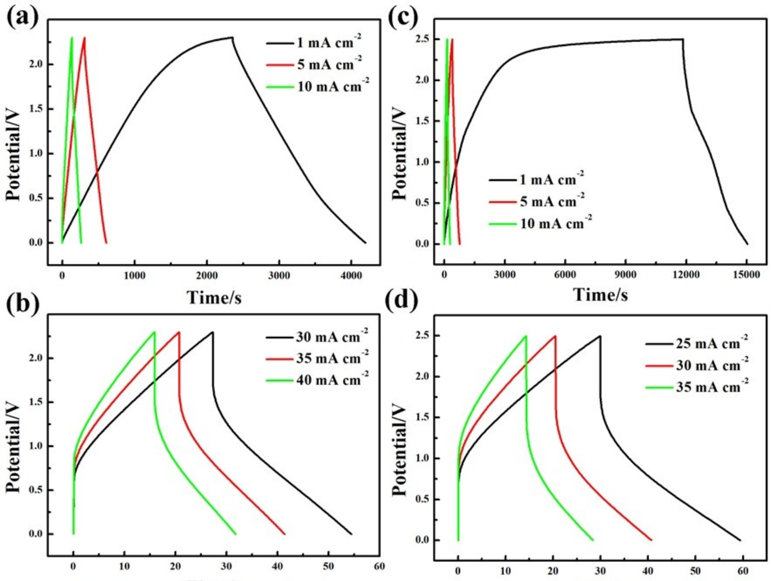

Fig. S14 (a, b) GCD curves of the 2.3 V ATDS@OCC//CC supercapacitor at different current densities. (c, d) GCD curves of the 2.5 V ATDS@OCC//CC supercapacitor at different current densities.

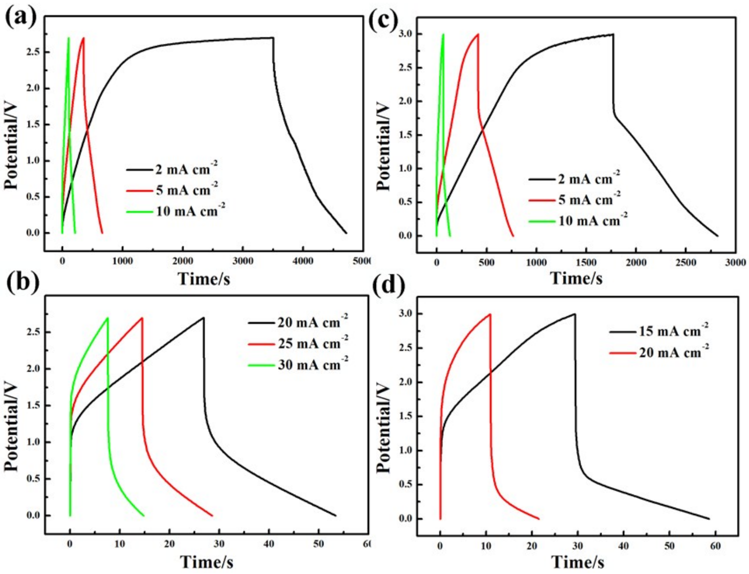

Fig. S15 (a, b) GCD curves of the 2.7 V ATDS@OCC//CC supercapacitor at different current densities. (c, d) GCD curves of the 3 V ATDS@OCC//CC supercapacitor at different current densities.

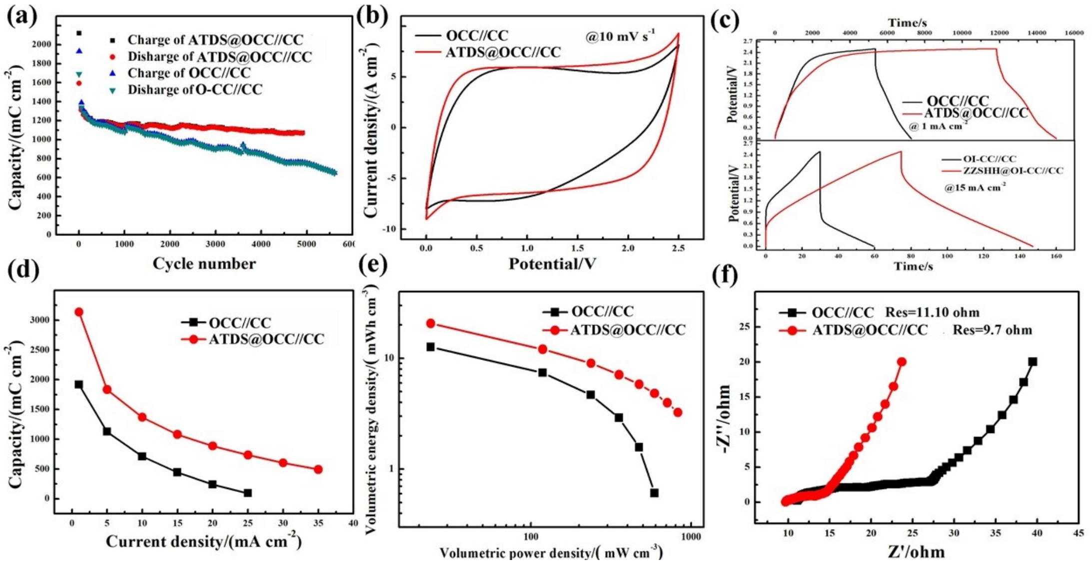

Fig. S16 Electrochemical properties of the OCC//CC and ATDS@OCC//CC aqueous supercapacitors with a voltage window of 0 V to 2.5 V. (a) Cycling stability at a current density of 18 mA cm^{-2}, (b) CV curves at 10 mV s^{-1}, (c) GCD curves at 1 and 15 mA cm^{-2}, (d) capacity as a function of current density, (e) Ragone plots and (f) Nyquist curves of the two supercapacitors after 13000 cycles.

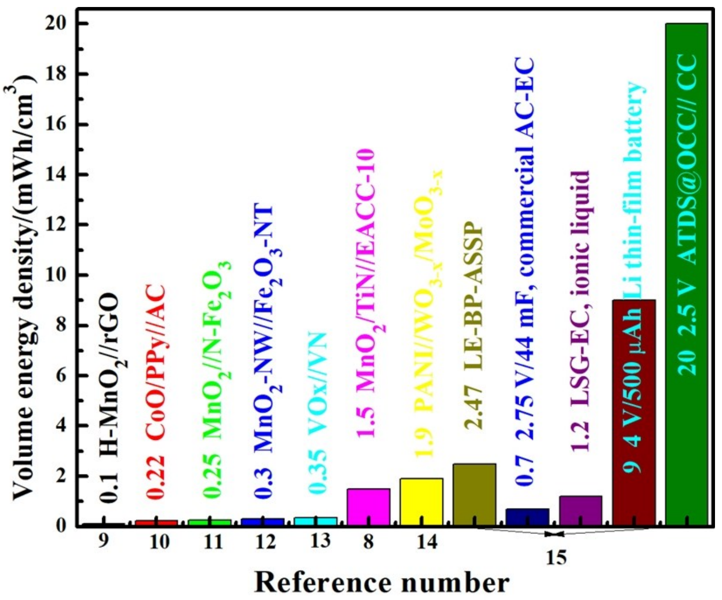

Fig. S17 Comparison of the volume energy density of ATDS@OCC//CC in this work with those reported in previous literatures. [8-17]

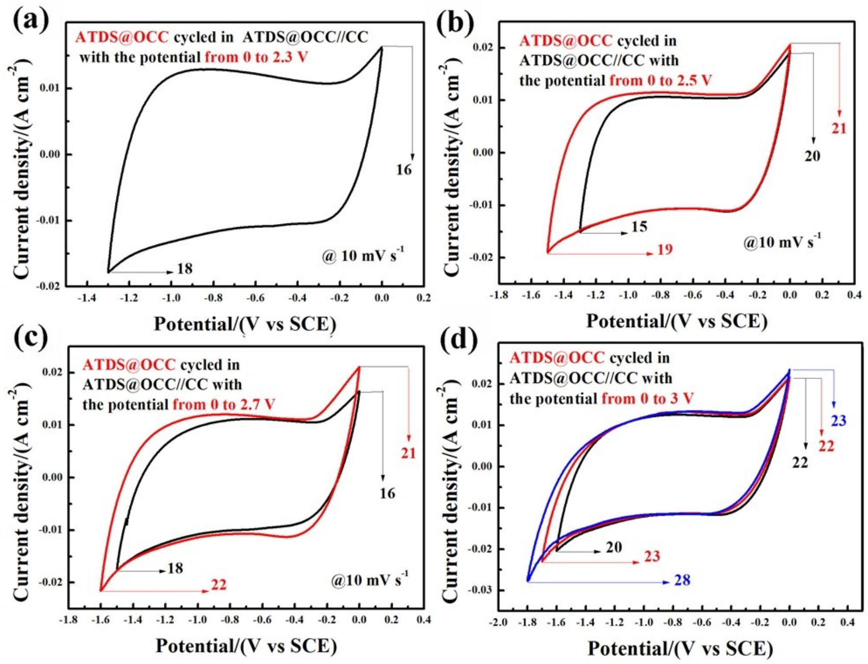

Fig. S18 CV curves of the cycled ATDS@OCC in ATDS@OCC//CC in the voltage windows of (a) 2.3 V, (b) 2.5 V, (c) 2.7 V and (d) 3 V.

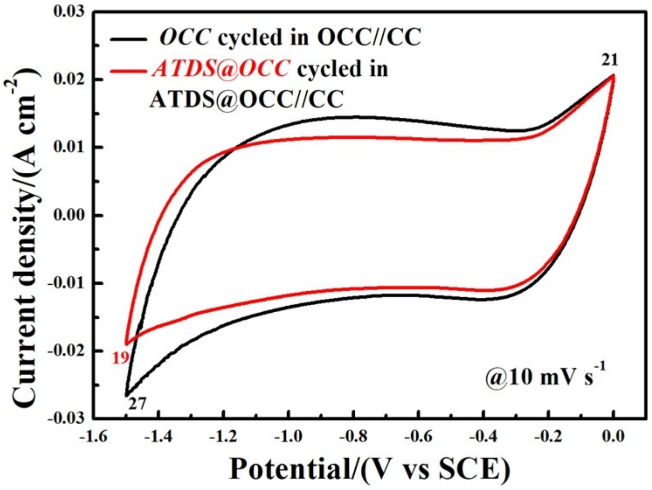

Fig. S19 CV curves of the cycled ATDS@OCC in ATDS@OCC//CC and the cycled OCC in OCC//CC in the voltage window of 2.5 V.

Table S1 Relative atom percentage on the surface of samples based on XPS results.

Samples	C/at%	N/at%	O/at%	K/at%
CC	79	8	13	
OCC	64	5	29	2

Note S1

The theoretical potential of di-hydrogen evolution in 2 M Li_2SO_4 aqueous electrolyte is -0.35 V *vs* SHE according to the following equations [3, 18]

$$E_{RHE}=E_{SHE}+0.0591\times pH,$$

$$E_{SHE}=E_m+E_r$$

in which E_{RHE} is 0 V. E_{RHE} and E_{SHE} are the reversible hydrogen electrode and the standard hydrogen electrode, respectively. E_m and E_r are the measured electrode potential *vs* Hg/Hg_2SO_4 and the reference electrode potential *vs* SHE, respectively. pH of 2 M Li_2SO_4 aqueous electrolyte is 6 and the potential of Hg/Hg_2SO_4 is 0.61 V (*vs* SHE).

In our work, the reference electrode is the saturated calomel electrode (SCE) with the electrode potential of 0.24 V *vs* SHE at 25 °C. The pH value of 1 M Na_2SO_4 aqueous electrolyte is about 6 measured by pH indicator paper. Thus, E_m is -0.59 V *vs* SCE.

Note S2

The mass loading of Zn in the total 7 mg cm^{-2} is estimated to be 3.20 mg cm^{-2}. The calculation is as followings. The mass ratio of Zn^0/Zn^{2+} is 1.71 based on the Zn2p narrow XPS spectra, and the ratio of Zn^{2+} in $Zn_4SO_4(OH)_6\cdot 4H_2O$ is 0.49 (260/530). The masses of Zn and $Zn_4SO_4(OH)_6\cdot 4H_2O$ are regarded as X and Y, respectively. Two equations can be listed based on the above,

$$X + Y = 7$$

$$Zn^0/Zn^{2+}=1.71=X/0.49Y$$ (mass ratio of Zn^0 and Zn^{2+})

Thus, X and Y equal to 3.20 and 3.80 mg cm^{-2}, respectively.

References

1. X. Leng, Y. Shao, L. Wu, S. Wei, Z. Jiang, G. Wang, Q. Jiang and J. Lian, *Journal of Materials Chemistry A*, 2016, **4**, 10304-10313.

2. J. Xu, M. Wang, N. P. Wickramaratne, M. Jaroniec, S. Dou and L. Dai, *Advanced materials*, 2015, **27**, 2042-2048.
3. Q. Gao, L. Demarconnay, E. Raymundo-Piñero and F. Béguin, *Energy & Environmental Science*, 2012, **5**, 9611.
4. K. Jurewicz, E. Frackowiak and F. Béguin, *Applied Physics A*, 2004, **78**, 981-987.
5. F. Béguin, K. Kierzek, M. Friebe, A. Jankowska, J. Machnikowski, K. Jurewicz and E. Frackowiak, *Electrochimica Acta*, 2006, **51**, 2161-2167.
6. A. Slesinski, C. Matei-Ghimbeu, K. Fic, F. Béguin and E. Frackowiak, *Carbon*, 2018, **129**, 758-765.
7. M. V. Lopez-Ramon, F. Stoeckli, C. Moreno-Castilla and F. Carrasco-Marin, *Carbon*, 1999, **37**, 1215-1221.
8. T. Zhai, S. Xie, M. Yu, P. Fang, C. Liang, X. Lu and Y. Tong, *Nano Energy*, 2014, **8**, 255-263.
9. C. Zhou, Y. Zhang, Y. Li and J. Liu, *Nano letters*, 2013, **13**, 2078-2085.
10. X. Lu, Y. Zeng, M. Yu, T. Zhai, C. Liang, S. Xie, M.-S. Balogun and Y. Tong, *Advanced materials*, 2014, **26**, 3148-3155.
11. M.-H. Bai, T.-Y. Liu, F. Luan, Y. Li and X.-X. Liu, *J. Mater. Chem. A*, 2014, **2**, 10882-10888.
12. T. Zhai, X. Lu, Y. Ling, M. Yu, G. Wang, T. Liu, C. Liang, Y. Tong and Y. Li, *Advanced materials*, 2014, **26**, 5869-5875.
13. Y.-H. Hwang, S. M. Lee, Y. J. Kim, Y. H. Kahng and K. Lee, *Carbon*, 2016, **100**, 7-15.
14. D. Chao, X. Xia, C. Zhu, J. Wang, J. Liu, J. Lin, Z. Shen and H. J. Fan, *Nanoscale*, 2014, **6**, 5691-5697.
15. C. Hao, B. Yang, F. Wen, J. Xiang, L. Li, W. Wang, Z. Zeng, B. Xu, Z. Zhao, Z. Liu and Y. Tian, *Advanced materials*, 2016, **28**, 3194-3201.
16. D. Zhao, C. Chen, Q. Zhang, W. Chen, S. Liu, Q. Wang, Y. Liu, J. Li and H. Yu, *Advanced Energy Materials*, 2017, **7**, 1700739.
17. C. Chen, Y. Zhang, Y. Li, J. Dai, J. Song, Y. Yao, Y. Gong, I. Kierzewski, J. Xie and L. Hu, *Energy & Environmental Science*, 2017, **10**, 538-545.
18. C. Wei, R. R. Rao, J. Peng, B. Huang, I. E. L. Stephens, M. Risch, Z. J. Xu and Y. Shao-Horn, *Advanced materials*, 2019, 1806296.